Engineered charge transport layers for improving indoor perovskite photovoltaic performance

Journal of Physics: Energy

PAPER

Engineered charge transport layers for improving indoor perovskite photovoltaic performance

Ram Datt[1], **Pietro Caprioglio**[2], **Saqlain Choudhary**[2], **Weixia Lan**[3], **Henry Snaith**[2,*] and **Wing Chung Tsoi**[1,*]

[1] SPECIFIC, Faculty of Science and Engineering, Swansea University, Bay Campus, Fabian Way, Swansea SA1 8EN, United Kingdom
[2] Department of Physics, University of Oxford, Clarendon Laboratory, Oxford OX1 3PU, United Kingdom
[3] School of Mechatronic Engineering and Automation, Shanghai University, Shanghai 200444, People's Republic of China
* Authors to whom any correspondence should be addressed.

E-mail: henry.snaith@physics.ox.ac.uk and w.c.tsoi@swansea.ac.uk

Keywords: perovskite solar cells, indoor photovoltaic, self-assembled monolayer, charge transport layers

OPEN ACCESS

RECEIVED
23 December 2023

REVISED
23 February 2024

ACCEPTED FOR PUBLICATION
8 March 2024

PUBLISHED
21 March 2024

Abstract

The developing Internet of Things market is attracting the indoor photovoltaic (IPV) as an essential power source. Perovskite photovoltaics (PPVs) are a fascinating candidate for IPV in solution-processable photovoltaics. Recent developments in PPVs can deliver power conversion efficiency (PCE) up to 25% outdoor (AM 1.5 G) and over 40% under indoor (1000 lux) light. The selection of charge transport layers (CTLs) has played an essential role in improving PPVs indoor performance. Herein, formamidinium-caesium-based mixed-cation ($FACsPb(I,Br)_3$) PPV devices are fabricated, and evaluated their outdoor and indoor performances by changing the different CTL combinations such as PTAA-PCBM and SAM-C_{60}. Outdoor PCEs were 13.76% and 15.27% achieved for PTAA-PCBM and SAM-C_{60}-based devices, respectively. Meanwhile, under LED (4000 K) 1000 lux, the PCEs were 26.32% and 31.92% for PTAA-PCBM and SAM-C_{60}-based PPV, respectively. The short circuit current (J_{sc}) (116.8–122.5 μA cm^{-2}) and fill factor (FF) (0.724–0.817) were the main parameters which improved for SAM-C_{60}-based devices under indoor light. This study points to the importance of CTL combination and indicates the promising potential of SAM-C_{60} interlayers in PPV indoor applications.

1. Introduction

Semiconducting perovskite (organic and inorganic hybrid) materials have revolutionized cost-effective photovoltaic development by showing their high absorption coefficient, long charge carrier diffusion length, and solution processability [1]. Most importantly, the band gap tunability of perovskite materials opens the applications for single junction, multiple junctions, and tandem photovoltaic fabrication with inorganic photovoltaic such as Cu(In, Ga)Se_2 (CIGS) and silicon solar cells [2–5]. The last decade of materials and devices development helped in improving the perovskite photovoltaics (PPV's) power conversion efficiency (PCE) from 9.7 to 25.7% for a single junction device under 1 sun (AM 1.5 G) [6, 7]. Interestingly, PPVs with wide band gaps and their high indoor light sensitivity showed a viable option for indoor application. Recent developments in PPVs for indoor showed an attractive PCE under 1000 lux [8]. PPVs are made of perovskite materials, charge transport layers (CTL) (hole and electron transport), and top and bottom electrodes. Adequate charge transportation and collection of photogenerated electrons and holes towards their respective electrodes are the main role played by CTL, and these also helps to reduce the charge carrier recombination's effectively at the interfaces [9]. The introduction of self-assembled monolayers (SAMs) as a CTL reduced interfacial charge-carrier recombination, provided efficient energy band alignment and it is now becoming a key component in PPVs fabrication [10]. The impact of interface engineering in PPVs has been well-reported in the literature [11–13]. Shin *et al* [14] studied the impact of inserting a polar bathocuproine (BCP) layer as an electron transport layer in a $CH_3NH_3PbI_3$ ($MAPbI_3$) perovskite-based device. It significantly improved the indoor PCE from 23.70 to 26.44% under 1000 lux (LED 6500k). The

prominent role of BCP is played via dipole-induced suppressed charge recombination and surface passivation. $MAPbI_3$ perovskite based indoor PPV devices have been studied with different material interlayers and delivered up to 39.2% of PCE under 1000 lux [15, 16]. Per literature, ∼1.9 eV wide band gap photovoltaic material is suggested under indoor light to achieve optimum PCE [17]. In perovskite, the mixed cations strategy has been proposed to tune the perovskite film band gap, and it also led to enhanced PPV device stability [18]. Caesium-based wide band gap mixed cation perovskite is known for structural stability, reduced trap-state density, low hysteresis behavior and also could delivered high open circuit voltage (V_{oc}) up to 1.29 V for 1.8 eV band gap perovskite system, under 1 sun AM 1.5 G [11, 19–21]. The replacement of MA^+ and iodide ions with FA^+ and Cs^+, and Br^- or Cl^-, respectively has improved thermal stability compared to the $MAPbI_3$ system [22, 23]. The mixed cations and mixed halides-based $FACsPb(Br,I)_3$ perovskite is a wide band gap system, and the band gap tunability achieved by varying Cs and Br [24, 25]. The $FACsPb(I,Br)_3$ also has the advantage of suppressing photo-induced halide segregation [26, 27]. The SAM-based $FACsPb(I,Br)_3$ PPV devices were studied under 1 Sun as well as under a concentrator (>10 sun) for outdoor application [28–30]. However, the study under indoor light is currently lacked.

In this work, we investigated the $FACsPb(I,Br)_3$ based PPV devices with two CTLs combinations called PTAA-PCBM and SAM-C_{60}. The device structure with PTAA-C_{60} CTLs has also been included. Their performance was evaluated under outdoor (1 sun AM 1.5 G) and indoor light (LED 200/1000 lux), respectively. We found that the CTLs can affect their performance significantly, with the SAM-C_{60} combination the PCE improved under outdoor and indoor conditions. Short circuit current (J_{sc}) and the fill factor (FF) were the main improved parameters.

2. Experimental

Glass substrates coated with patterned indium-doped tin oxide (Biotain Crystal Co., 10–15 ohm sq^{-1}) were washed with Hellmanex III, deionised (DI) water, acetone, and isopropanol. After UV-O_3 treatment (15 min for PTAA and 30 min for SAM), poly[bis(4-phenyl) (2,4,6-trimethylphenyl) amine] (PTAA) in a concentration of 1.5 mg ml^{-1} in Toluene was spin-coated at 6000 rpm for 30 s and immediately annealed for 10 min at 100 °C under N_2 atmosphere. Alternatively, a Me4-PACz (Tokyo Chemical Industry) solution 0.3 mg ml^{-1} in Ethanol was spin-coated at 2000 rpm for 30 s and immediately annealed for 10 min at 100 °C. The PTAA was additionally treated by dynamically spin coating a diluted solution (0.5 mg ml^{-1} in methanol) of poly[(9,9-bis(30-((N,Ndimethyl)- N-ethylammonium)-propyl)–2,7 fluorene)-alt-2,7-(9,9-dioctylfluorene)]dibromide (PFN-P2). The SAM layer was additionally treated with a solution of Al_2O_3 nanoparticles diluted at 1:150 by volume in IPA spin-coated using the same parameters of the PFN deposition.

The composition of the perovskite was $FA_{0.83}Cs_{0.17}Pb(I_{0.6}Br_{0.4})_3$. This was made by dissolving: 371.46 mg of Formamidinium Iodide (Greatcell, 99.99% purity), 114.8 mg of Caesium Iodide (TCI, 99.99% purity), 774.5 mg of Lead Iodide (TCI, 99.9% purity) and 578.3 mg of Lead Bromide (TCI, 99.99% purity) in 2.4 ml of 4:1 DMF:DMSO. The perovskite layer was formed by spin coating a DMF:DMSO solution (4: 1 volume) starting at 1000 rpm for 5 s (ramping time of 5 s from stationary status) and then 5000 rpm (ramping time of 5 s from 1000 rpm) for 30 s. Before the end of the spinning process, a solvent-quenching method was used by dropping ethyl acetate (300 μl) onto the spinning substrates at 40 s after the start of the spin-coating process.

A phenylC_{61}-butyric acid methyl ester (PCBM) solution (20 mg ml^{-1} in CB:DCB 9:1 by volume) was dynamically spun onto the perovskite layers at a speed of 2000 rpm for 20 s. The samples were then annealed at 100 °C for 3–5 min. After cooling down to room temperature, a BCP solution (0.5 mg ml^{-1} in IPA) was dynamically spun onto the PCBM layer at a speed of 4000 rpm for 20 s, followed by a brief thermal annealing process at 100°C for ∼1 min. Both PCBM and BCP were processed inside the nitrogen-filled glovebox. For the C_{60} devices, 20 nm of C_{60} was evaporated followed by 5 nm of BCP. The hybrid perovskite single-junction solar cells were completed by thermal evaporation of Silver (Ag) (Nano 36, Kurt J. Lesker) electrode (100 nm) through shadow masks under high vacuum (6×10^{-6} torr) using a thermal evaporator. The device pixel area was 0.3087 cm^2.

The device with PTAA and PCBM was assigned as PTAA-PCBM, and the device with SAM and C_{60} was named as SAM-C_{6O} devices, and their structures are shown in figures 1(a) and (b), respectively.

3. Characterization

Keithley 2420 source meter and Newport solar simulator (Model no. 94023A) have been used to characterize photovoltaic properties under 1 sun AM 1.5 G, and the standard silicon solar cells were used to calibrate sun light. A QE X10 (PV measurement) system is used to measure the external quantum efficiency (EQE). The indoor measurement was conducted using an LED 4000 K bulb box under 1000 lux and 200 lux light

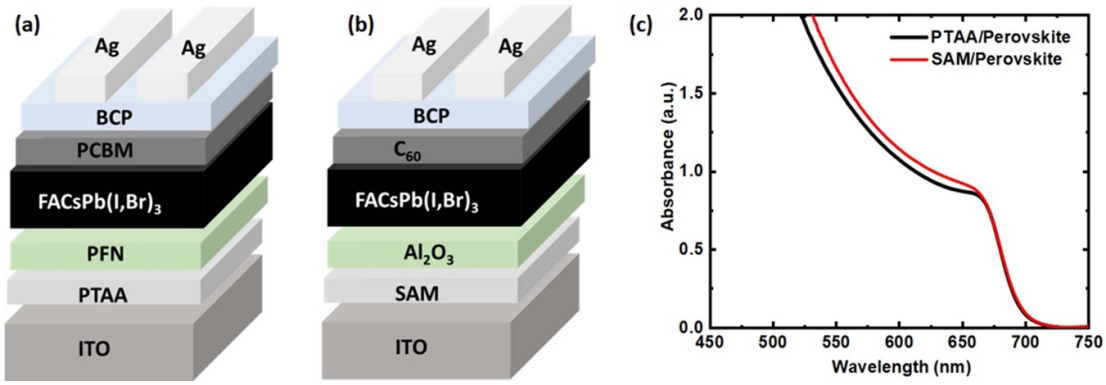

Figure 1. Device structures for the (a) PTAA-PCBM and (b) SAM-C_{60}-based PPV, (c) Absorption spectra of spin-coated perovskite layers on top of SAM or PTAA thin film.

illuminations. The LED light spectrum and indoor light box are shown in figures S1 and S2 in supporting information, respectively.

4. Results and discussion

Figure 1(c) shows the absorption spectra of $FACsPb(I,Br)_3$ perovskite film coated on top of the PTAA and SAM layer. The $FACsPb(I,Br)_3$ showed absorption in the visible region, indicating a promising layer for preparing PPV for indoor application. Figures 2(a) and (b) show the current density–voltage (J-V) characteristics of PTAA-PCBM and SAM-C_{60} devices measured under 1 sun AM 1.5 G. PTAA-PCBM device showed V_{oc}, J_{sc}, and FF of 1.17 V, 16.13 mA cm^{-2}, and 0.7351, respectively, and delivered PCE up to 13.67% under forward scan. Meanwhile, the SAM-C_{60} device under forward scan showed V_{oc}, J_{sc}, and FF of 1.17 V, 17.68 mA cm^{-2}, and 0.7328, respectively, and delivered PCE up to 15.15%. The J_{sc} for both types of devices were well-matched with the EQE integrated current density (J_{EQE}). The EQE spectra are shown in figures 2(c) and (d) for PTAA-PCBM and SAM-C_{60}-based PPV devices, respectively. The calculated J_{EQE} were 16.06 and 17.20 mA cm^{-2} for PTAA-PCBM and SAM-C_{60}-based PPV devices, respectively, and the differences in current density calculated from J–V and EQE were under 2%. The SAM-C_{60} device showed improvement in J_{sc}, whereas the FF and V_{oc} parameters appear similar. Moreover, the SAM-C_{60}-based PPV devices showed low hysteresis compared to PTAA-PCBM devices. The photovoltaic parameters for both types of devices are summarized in table 1. In the figure 1(a) device structure, the PCBM layer has also been replaced by C_{60} and the corresponding device called PTAA-C_{60}. The device delivered photovoltaic parameters V_{oc}, J_{sc}, and FF, and PCE of 1.15 V, 17.28 mA cm^{-2}, 0.721, and 14.40%, respectively. The J_{sc} is well matched with J_{EQE} (17.21 mA cm^{-2}) and showed low hysteresis. Figures S5 and S6 (supporting information) show the J–V characteristics and EQE plot.

Figures 3(a) and (b) show the J–V characteristics (figures S3 and S4 contains forward and reverse scan JV) of PTAA-PCBM and SAM-C_{60}-based PPV devices measured under indoor light, and the calculated photovoltaic parameters are summarized in table 2. Under 1000 lux, the PTAA-PCBM device delivered V_{oc}, J_{sc}, FF, and PCE of 0.990 V, 116.83 μA cm^{-2}, 0.724, and 26.32%, respectively. Whereas, under 200 lux, the photovoltaic parameters V_{oc}, J_{sc}, FF, and PCE were 0.921 V, 24.3 μA cm^{-2}, 0.690, and 24.40%, respectively. The SAM-C_{60}-based device under 1000 lux has V_{oc}, J_{sc}, FF, and PCE of 0.996 V, 122.5 μA cm^{-2}, 0.817, and 31.92%, respectively. Whereas under 200 lux, V_{oc}, J_{sc}, FF, and PCE were 0.934 V, 24.5 μA cm^{-2}, 0.798, and 29.32%. The SAM-C_{60}-based PPV improved performance compared to PTAA-PCBM devices under 1000 lux and 200 lux. The PCE improved from 26.32 to 31.92% and from 24.40 to 29.32% under 1000 lux and 200 lux, respectively. The main improved parameters were FF (0.724–0.817) and J_{sc} (116.83–122.5 mA cm^{-2}). The EQE spectra are also used to calculate the J_{EQE} under low light illumination. At 1000 lux, the J_{EQE} were 113.68 and 120.49 μA cm^{-2} for PTAA-PCBM and SAM-C_{60} devices, respectively. The difference in J_{sc} and J_{EQE} is under 2%, and it shows the reliability of the indoor measurement. The PTAA-C_{60} device showed PCE of 30.41 and 28.70% under 1000 and 200 lux, respectively. The performance is lower than SAM-C_{60}-based PPV under indoor light. Meanwhile, PTAA-C_{60} devices show low hysteresis under indoor light. Figures S7 and S8 (supporting information) show the PTAA-C_{60} device's J–V characteristics under indoor light.

The charge carrier recombination suppression was investigated for PTAA-PCBM, and SAM-C_{60}-based devices by studying the voltage and current dependence on light intensity (100–1 mW cm^{-2}). Different light intensity is achieved by using neutral density filters. The power law J_{sc} dependency with light intensity

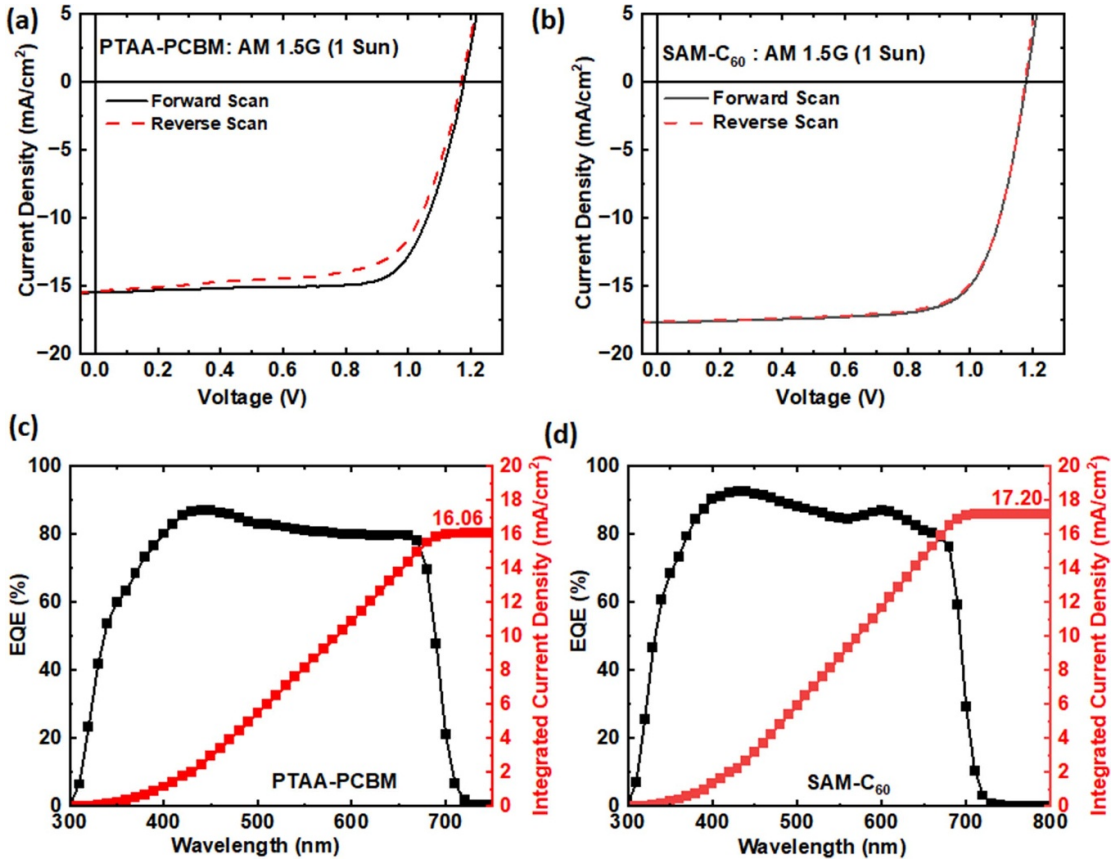

Figure 2. *J–V* characteristics under AM 1.5 G of (a) PTAA-PCBM and (b) SAM-C_{60} interlayers- based PPV. EQE plots with calculated J_{EQE} values of (c) PTAA-PCBM and (d) SAM-C_{60}-based PPV devices.

Table 1. Photovoltaic performance parameters of PTAA-PCBM and SAM-C_{60}-based PPV devices measured under AM 1.5 G (100 mW cm^{-2}).

Device	Scan	V_{oc} (V)	J_{sc} (mA cm^{-2})	J_{EQE} (mA cm^{-2})	FF (%)	PCE (%)
PTAA-PCBM	Forward	1.16 ± 0.0017 (1.17)	15.50 ± 0.44 (16.13)	16.06	73.17 ± 0.23 (73.51)	13.40 ± 0.25 (13.76)[a]
	Reverse	1.15 ± 0.009 (1.16)	15.52 ± 0.41 (16.11)		63.88 ± 2.35 (67.21)	11.89 ± 0.20 (12.19)[a]
SAM-C_{60}	Forward	1.16 ± 0.010 (1.17)	17.5 ± 0.14 (17.68)	17.20	72.37 ± 0.91 (73.28)	14.91 ± 0.24 (15.15)[a]
	Reverse	1.16 ± 0.007 (1.17)	17.4 ± 0.18 (17.66)		72.5 ± 0.36 (72.9)	14.79 ± 0.27 (15.06)[a]

[a] Calculated from four devices.

(I_{light})) by $J_{sc} \propto I_{light}^{\alpha}$ relation, where α is a recombination parameter [31]. Figure 4(a), plotted on a log-log scale, show the power law fitted data of PTAA-PCBM and SAM-C_{60}-based PPV devices. The exponent (α) values of PTAA-PCBM and SAM-C_{60} devices were 0.985 and 0.995, respectively. The SAM-C_{60} device has α value close to 1, implying reduced bimolecular recombination [32]. The impact is reflected in improving the J_{sc} and FF of SAM-C_{60}-based devices. The slope kT/q, where k, T, and q are the Boltzmann constant, temperature (in Kelvin), and elementary charge, respectively. It calculated from light intensity dependent V_{oc} using following law of $V_{oc} \propto \frac{nKT}{q} InI_{light}$. The deviation of slope from 1 KT/q shows the probability of trap-induced recombination at open circuit condition [32]. The slopes are 1.47 KT/q and 1.42 KT/q (figure 4(b)) for the PTAA-PCBM and the SAM-C_{60}-based devices. A lower slope value suggested the reduction of trap-assisted recombination. Changing the CTL can reduce trap-assisted recombination in the PPV under open conditions. As a result, the device's outdoor and indoor performance has improved. The SAM-C_{60} device shows FF, V_{oc} and J_{sc} higher than PTAA-PCBM-based PPV under indoor light.

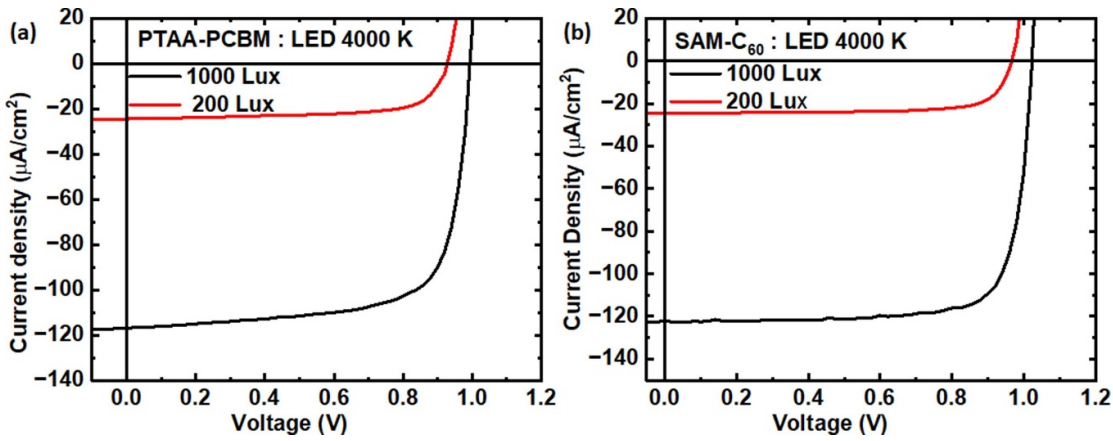

Figure 3. *J–V* characteristics of (a) PTAA-PCBM and (b) SAM-C_{60}-based PPV under LED 1000 and 200 lux indoor lights.

Table 2. Photovoltaic performance parameters of PTAA-PCBM and SAM-C_{60}-based PPV devices measured under indoor light (LED 4000 K).

Device	Illuminance (Lux)	Irradiance (μW cm^{-2})	Scan	V_{oc} (V)	J_{sc} (μA cm^{-2})	J_{EQE} (μA cm^{-2})	FF (%)	PCE (%)
PTAA-PCBM	1000	312.7	Forward	0.988 ± 0.0059 (0.990)	116.16 ± 0.67 (116.83)	113.68	72.01 ± 0.46 (72.47)	26.05 ± 0.27 (26.32)
	200	62.6	Forward	0.918 ± 0.003 (0.921)	24.07 ± 0.21 (24.3)		68.32 ± 0.73 (69.05)	23.83 ± 0.57 (24.40)
SAM-C_{60}	1000	312.7	Forward	0.991 ± 0.0049 (0.996)	122.07 ± 0.43 (122.5)	120.49	81.24 ± 0.51 (81.75)	30.86 ± 1.06 (31.92)
	200	62.6	Forward	0.929 ± 0.0045 (0.934)	24.18 ± 0.32 (24.5)		79.44 ± 0.43 (79.87)	28.17 ± 1.15 (29.32)

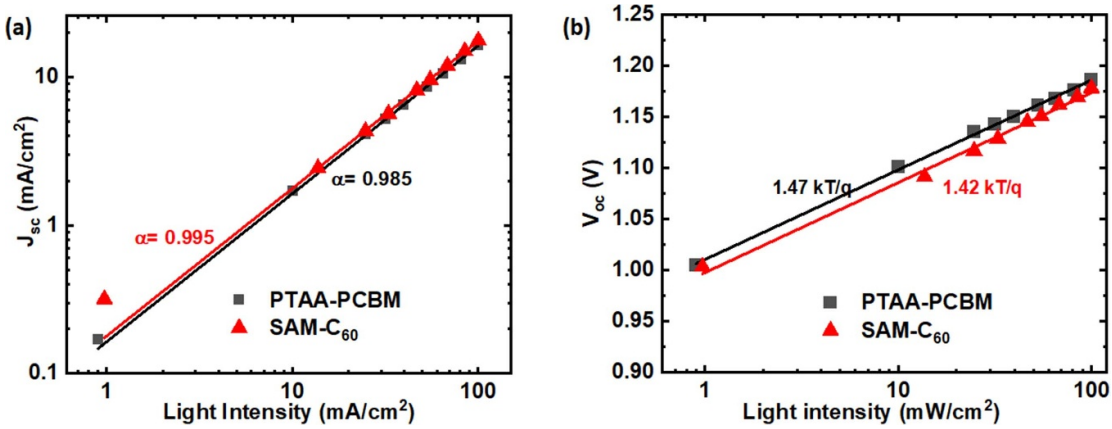

Figure 4. (a) J_{sc} vs light intensity plots of PTAA-PCBM and SAM-C_{60}-based PPV. (b) V_{oc} versus light intensity plots of PTAA-PCBM and SAM-C_{60}-based PPV.

5. Conclusions

In conclusion, caesium-based mixed-cation and mixed halide perovskites ($FACsPb(I,Br)_3$) based PPV devices were fabricated and studied under outdoor and indoor light conditions. The significance of selecting the suitable CTL for indoor PPV fabrication has been discussed. The AM 1.5 G (1 sun) PCE of PTAA-PCBM-based PPV is 13.76% which is improved to 15.06% for SAM-C_{60}-based PPV (9.45% enhancement in PCE). Notably, the PCE under 1000 lux for PTAA-PCBM-based PPV is 26.32%, which is more significantly improved to 31.92% for SAM-C_{60}-based PPV (21.3% enhancement in PCE). The J_{sc} and FF were the main photovoltaic parameters that improved indoor performance. The J_{sc} and V_{oc}-dependent, light intensity measurement suggested the reduced biomolecular and trap-assisted recombination in

SAM-C_{60}-based PPV. The recombination parameter and ideality factor improved from 0.985 (PTAA-PCBM) to 0.995 (SAM-C_{60}), and 1.47 (PTAA-PCBM) to 1.42 (SAM-C_{60}). This study suggested the significance of CTL selection for increasing PPV device indoor performance. The PTAA-C_{60} CTLs also show a potential for indoor PPV as the device delivered PCE of 30.41% under 1000 lux. Furthermore, PTAA-C_{60} devices showed low hysteresis under indoor light. C_{60} works well with SAM and PTAA layers for indoor PPV.

Data availability statement

All data that support the findings of this study are included within the article (and any supplementary files).

Acknowledgments

R D sincerely acknowledges the SPECIFIC Innovation and Knowledge Centre (EP/N020863/1). W C T, H S, R D and P C acknowledged Engineering and Physics Science Research Council (EPSRC) Application Targeted And Integrated Photovoltaics (ATIP) (EP/T028513/1) Grant for providing financial support. W C T and W L would like to acknowledge the Foreign Expert Foundation of China funding (G2023013014L).

Conflict of interest

The authors declare no conflict of interest.

ORCID iDs

Ram Datt https://orcid.org/0000-0003-3109-1278
Pietro Caprioglio https://orcid.org/0000-0002-3465-2475
Saqlain Choudhary https://orcid.org/0000-0002-6567-3121
Weixia Lan https://orcid.org/0000-0003-0580-1715
Henry Snaith https://orcid.org/0000-0001-8511-790X
Wing Chung Tsoi https://orcid.org/0000-0003-3836-5139

References

[1] Park N-G 2015 Perovskite solar cells: an emerging photovoltaic technology *Mater. Today* **18** 65–72
[2] Fang Z *et al* 2021 Perovskite-based tandem solar cells *Sci. Bull.* **66** 621–36
[3] Zhang Z, Li Z, Meng L, Lien S and Gao P 2020 Perovskite-based tandem solar cells: get the most out of the Sun *Adv. Funct. Mater.* **30** 2001904
[4] Aydin E *et al* 2023 Enhanced optoelectronic coupling for perovskite/silicon tandem solar cells *Nature* **623** 732–8
[5] Jošt M *et al* 2022 Perovskite/CIGS Tandem solar cells: from certified 24.2% toward 30% and beyond *ACS Energy Lett.* **7** 1298–307
[6] Kim H-S *et al* 2012 Lead iodide perovskite sensitized all-solid-state submicron thin film mesoscopic solar cell with efficiency exceeding 9% *Sci. Rep.* **2** 591
[7] Kim M *et al* 2022 Conformal quantum dot–SnO_2 layers as electron transporters for efficient perovskite solar cells *Science* **375** 302–6
[8] He X, Chen J, Ren X, Zhang L, Liu Y, Feng J, Fang J, Zhao K and Liu S (Frank) 2021 40.1% record low-light solar-cell efficiency by holistic trap-passivation using micrometer-thick perovskite film *Adv. Mater.* **33** 2100770
[9] Cheng M, Zuo C, Wu Y, Li Z, Xu B, Hua Y and Ding L 2020 Charge-transport layer engineering in perovskite solar cells *Sci. Bull.* **65** 1237–41
[10] Al-Ashouri A, Köhnen E, Li B, Magomedov A, Hempel H, Caprioglio P, Márquez J A, and Morales Vilches A B 2020. Monolithic perovskite/silicon tandem solar cell with >29% efficiency by enhanced hole extraction *Science* **370** 1300–09
[11] Caprioglio P *et al* 2023 Open-circuit and short-circuit loss management in wide-gap perovskite p-i-n solar cells *Nat. Commun.* **14** 932
[12] Caprioglio P *et al* 2021 Bi-functional interfaces by poly(ionic liquid) treatment in efficient pin and nip perovskite solar cells *Energy Environ. Sci.* **14** 4508–22
[13] Pan H *et al* 2020 Advances in design engineering and merits of electron transporting layers in perovskite solar cells *Mater. Horiz.* **7** 2276–91
[14] Shin S J, Alosaimi G, Choi M J, Ann M H, Jeon G G, Seidel J, Kim J, Yun J S and Kim J H 2022 Strategic approach for frustrating charge recombination of perovskite solar cells in low-intensity indoor light: insertion of polar small molecules at the interface of the electron transport layer *ACS Appl. Energy Mater.* **5** 13234–42
[15] Choi M J *et al* 2023 Strategic approach for achieving high indoor efficiency of perovskite solar cells: frustration of charge recombination by dipole induced homogeneous charge distribution *Chem. Eng. J.* **454** 140284
[16] Li N, Feng A, Guo X, Wu J, Xie S, Lin Q, Jiang X, Liu Y, Chen Z and Tao X 2022 Engineering the hole extraction interface enables single-crystal $MAPbI_3$ perovskite solar cells with efficiency exceeding 22% and superior indoor response *Adv. Energy Mater.* **12** 2103241
[17] Hou X *et al* 2020 Indoor application of emerging photovoltaics—progress, challenges and perspectives *J. Mater. Chem. A* **8** 21503–25
[18] Xu F, Zhang T, Li G and Zhao Y 2017 Mixed cation hybrid lead halide perovskites with enhanced performance and stability *J. Mater. Chem.* A **5** 11450–61
[19] Salado M, Kazim S and Ahmad S 2018 The role of Cs+ inclusion in formamidinium lead triiodide-based perovskite solar cell *Chem. Pap.* **72** 1645–50

[20] Sun X et al 2022 Highly efficient $CsPbI_3/Cs_{1-x}DMA_xPbI_3$ bulk heterojunction perovskite solar cell *Joule* **6** 850–60
[21] Guo Q, Ding Y, Dai Z, Chen Z, Du M, Wang Z, Gao L, Duan C, Guo Q and Zhou E 2022 Multiple-cation wide-bandgap perovskite solar cells grown using cesium formate as the Cs precursor with high efficiency under sunlight and indoor illumination *Phys. Chem. Chem. Phys.* **24** 17526–34
[22] Akbulatov A F, Yu L S, Frolova L A, Dremova N N, Gerasimov K L, Zhidkov I S, Anokhin D V, Kurmaev E Z, Stevenson K J and Troshin P A 2017 Probing the intrinsic thermal and photochemical stability of hybrid and inorganic lead halide perovskites *J. Phys. Chem. Lett.* **8** 1211–8
[23] Ouedraogo N A N, Chen Y, Xiao Y Y, Meng Q, Han C B, Yan H and Zhang Y 2020 Stability of all-inorganic perovskite solar cells *Nano Energy* **67** 104249
[24] Tregnago G 2018 Perovskites tower up *Nat. Energy* **3** 709
[25] Tan W, Bowring A R, Meng A C, McGehee M D and McIntyre P C 2018 Thermal stability of mixed cation metal halide perovskites in air *ACS Appl. Mater. Interfaces* **10** 5485–91
[26] Rehman W, McMeekin D P, Patel J B, Milot R L, Johnston M B, Snaith H J and Herz L M 2017 Photovoltaic mixed-cation lead mixed-halide perovskites: links between crystallinity, photo-stability and electronic properties *Energy Environ. Sci.* **10** 361–9
[27] Oliver R D J et al 2022 Understanding and suppressing non-radiative losses in methylammonium-free wide-bandgap perovskite solar cells *Energy Environ. Sci.* **15** 714–26
[28] Troughton J, Gasparini N and Baran D 2018 $Cs_{0.15}FA_{0.85}PbI_3$ perovskite solar cells for concentrator photovoltaic applications *J. Mater. Chem.* A **6** 21913–7
[29] Gil-Escrig L, Dreessen C, Palazon F, Hawash Z, Moons E, Albrecht S, Sessolo M and Bolink H J 2021 Efficient wide-bandgap mixed-cation and mixed-halide perovskite solar cells by vacuum deposition *ACS Energy Lett.* **6** 827–36
[30] Hsu H-C, Wu S-H, Tung Y-L and Shih C-F 2022 Long-term stable perovskite solar cells prepared by doctor blade coating technology using bilayer structure and non-toxic solvent *Org. Electron.* **101** 106400
[31] Singh T and Miyasaka T 2018 Stabilizing the efficiency beyond 20% with a mixed cation perovskite solar cell fabricated in ambient air under controlled humidity *Adv Energy Mater.* **8** 1700677
[32] Liu C, Tu J, Hu X, Huang Z, Meng X, Yang J, Duan X, Tan L, Li Z and Chen Y 2019 Enhanced hole transportation for inverted tin-based perovskite solar cells with high performance and stability *Adv. Funct. Mater.* **29** 1808059